NASA Technical Memorandum 100833

# Electromagnetic Propagation in PEC and Absorbing Curved S-Ducts

Kenneth J. Baumeister
*Lewis Research Center*
*Cleveland, Ohio*



Prepared for the
1988 IEEE AP-S International Symposium and URSI Radio Science Meeting
Syracuse, New York, June 6–10, 1988

NASA

# ELECTROMAGNETIC PROPAGATION IN PEC AND ABSORBING CURVED S-DUCTS

Kenneth J. Baumeister
National Aeronautics and Space Administration
Lewis Research Center
Cleveland, Ohio 44135

E-3507

## SUMMARY

A finite-element Galerkin formulation has been developed to study transverse magnetic (TM) wave propagation in two-dimensional S-curved ducts with both perfectly conducting and absorbing walls. The reflection and transmission at the entrances and the exits of the curved ducts are determined by coupling the finite-element solutions in the curved ducts to the eigenfunctions of an infinite, uniform, perfectly conducting duct. Example solutions are presented for a double mitred and S-ducts of various lengths. The length of the S-duct is found to significantly effect the reflective characteristics of the duct. Also, the effect of curvature on an absorbing duct wall is illustrated.

## INTRODUCTION

Electromagnetic propagation in curved ducts (wave guides) plays an important role in many practical physical systems. In microwave power generation systems for example (ref. 1, pp. 315-317), bends or corners are required to alter the direction of the wave. Since curves or corners represent discontinuities, reflection from the bends can be significant. To better understand the electromagnetic transmission properties of a bend, a finite-element Galerkin formulation has been developed to study wave propagation in curved S-shaped ducts. Both perfectly conducting and absorbing walls will be considered.

## NOMENCLATURE

| | |
|---|---|
| $A_n^+$ | mode amplitude of positive going entrance waves, equation (15) |
| $A_n^-$ | mode amplitude of reflected negative going entrance waves, equation (15) |
| $B_n^+$ | mode amplitude of positive going exit waves, equation (18) |
| $b'$ | characteristic duct height |
| $b_a$ | dimensionless entrance height $b_a'/b'$ |
| $b_b$ | dimensionless exit height $b_b'/b'$ |
| $c_o'$ | speed of light in vacuum |
| $\bar{E}$ | dimensionless harmonic electric field vector, $\sqrt{\frac{\varepsilon_o'}{\mu_o'}}\frac{\bar{E}'(x',y',z')}{H_o'}$ |
| $e_x,e_y,e_z$ | unit vectors in coordinate directions |
| $f$ | dimensionless frequency, equation (7) |

| | |
|---|---|
| $H$ | dimensionless harmonic magnetic intensity vector, $H'(x,y,z)/H'_o$ |
| $H_x$ | x component of magnetic intensity H |
| $H_{xi}$ | magnetic intensity at node i |
| $H'_o$ | normalizing magnitude of magnetic intensity |
| $\tilde{H}_x$ | finite-element approximation to $H_x$ |
| $j$ | $\sqrt{-1}$ |
| $k$ | wave number, $\omega/c$ |
| $k_{zn}$ | axial modal wave number, equations (16) and (17) |
| $L$ | dimensionless length, $L'/b'$ |
| $M$ | number of elements |
| $m$ | mode number, equation (20) |
| $N$ | number of nodes |
| $N_m$ | number of modes |
| $N_1, N_2, N_3$ | local interpolation shape functions |
| $n$ | mode number, equation (15) |
| $\bar{n}$ | outward normal unit vector |
| $S$ | length of line segment on boundary |
| $t$ | dimensionless time, $\frac{c'_o}{b'} t'$ |
| $W_i$ | weight, equation (25) |
| $x$ | dimensionless transverse distance, $x'/b'$ |
| $y$ | dimensionless transverse distance, $y'/b'$ |
| $z$ | dimensionless axial distance, $z'/b'$ |
| $\varepsilon_r$ | dielectric constant, $\varepsilon'/\varepsilon'_o$ |
| $\varepsilon_a$ | dielectric constant in entrance duct, $\varepsilon'_a/\varepsilon'_o$ |
| $\varepsilon'$ | permittivity |
| $\varepsilon'_o$ | permittivity in vacuum |
| $\varepsilon$ | complex permittivity, equation (5) |

$\mu_r$ relative permeability, $\mu'/\mu'_o$

$\mu'$ dimensional permeability

$\mu'_o$ permeability in vacuum

$\sigma$ dimensionless conductance, $\sigma' b'/c'_o \varepsilon'_o$

$\omega'$ angular velocity

$\omega$ dimensionless angular velocity, $\omega' b'/c'_o$

Subscripts

a entrance region

b exit region

x,y,z scalar vector components

Superscripts

(1) region 1

(2) region 2

' dimensional quantity

T transpose

- vector quantity

## GEOMETRICAL MODEL

In the finite-element modeling of the curved ducts to be presented, an S-shaped profile has been closed to approximate the two-dimensional cross-sectional profile that might be found in a typical bend, as shown in figure 1. The S-shaped profile can be prescribed by a simple third-degree polynomial of the form

$$y = 3\left(\frac{z}{L}\right)^2 - 2\left(\frac{z}{L}\right)^3 \tag{1}$$

where the dimensionless duct coordinates are defined as

$$y = \frac{y'}{b'_a} \quad z = \frac{z'}{b'_a} \quad L = \frac{L'}{b'_a} \tag{2}$$

and $b'_a$ is the height of the straight entrance duct leading into the curved duct. The S-curve defined by equation (1) has zero slope at z/L of 0 and 1;

providing a smooth transition from a straight entrance to the curved test section. In the foregoing equations, the prime, ', is used to denote a dimensional quantity and the unprimed defines a dimensionless quantity. This convention will be used throughout this paper. These and all other symbols used in the report are defined in the nomenclature.

This paper will focus on the interaction of a propagating duct mode traveling down the uniform entrance duct with the curved wall as shown in figure 2. The reflection and transmission at the entrance and exit of the curved duct are determined by coupling the finite-element solutions in the curved duct to the eigenfunctions of the infinite, uniform, perfectly conducting entrance and exit ducts. This permits a multimodal representation accounting for reflection and mode conversion by the nonuniformity (ref. 2).

## GOVERNING EQUATIONS

The governing differential equations are the standard Maxwell's equations along with the boundary conditions associated with perfectly conducting and lossy walls. Maxwell's equations will be combined to form a single wave equation for transverse magnetic wave propagation in a two-dimensional duct.

### Maxwell's Equations

Maxwell's curl equations for time harmonic ($e^{+j\omega t}$) variations in the electromagnetic fields are

$$\nabla \times \bar{E} = -j\omega\mu_r \bar{H} \tag{3}$$

$$\nabla \times \bar{H} = j\omega\varepsilon \bar{E} \tag{4}$$

where the total permittivity included conduction

$$\varepsilon = \varepsilon_r - j\sigma/\omega \tag{5}$$

$$\sigma = \frac{\sigma' b'_a}{c'_o \varepsilon'_o} \tag{6}$$

and the dimensionless frequency is defined as

$$f = \frac{f' b'_a}{c'_o} \qquad \omega = \frac{\omega' b'_a}{c'_o} \qquad \omega = 2\pi f \tag{7}$$

### Heterogeneous Variable Property Wave Equation

The number of dependent variables can be reduced by combining Maxwell's equations (3) and (4) into a single wave equation. It is desirable to develop a wave equation that could be used for varying media properties so that no special treatment of the interface between materials is required. That is,

the same equations apply in the duct and in the absorber region and only the material properties are changed.

Rewriting equation (4),

$$\frac{\nabla x \bar{H}}{j\omega\varepsilon} = \bar{E} \tag{8}$$

and taking the curl

$$\nabla x \left[ \frac{\nabla x \bar{H}}{j\omega\varepsilon} \right] = \nabla x \bar{E} \tag{9}$$

The constants $j\omega$ are independent of space and can be pulled out the curl operator in equation (9); however, $\varepsilon$ must remain inside since $\varepsilon$ is now assumed a function of the spatial dimensions.

$$\frac{1}{j\omega} \nabla x \left[ \frac{\nabla x \bar{H}}{\varepsilon} \right] = \nabla x \bar{E} \tag{10}$$

Substituting equation (10) into equation (3) yields our heterogeneous governing wave equation.

$$\nabla x \left[ \frac{\nabla x \bar{H}}{\varepsilon} \right] - \omega^2 \mu_r \bar{H} \tag{11}$$

## TM Variable Property Two-Dimensional Wave Equation

Transverse magnetic (TM) waves will now be assumed to represent the input electromagnetic modes propagating down the entrance duct towards the curved S-duct. For this two-dimensional geometry, the assumption is made that only one component of the $\bar{H}$ vector will exist in the problem domain, that is,

$$\bar{H}(y,z) = H_x(y,z)e_x \tag{12}$$

where $e_x$ is a unit vector in the $x$ direction (into the paper as shown in fig. 2). The magnitude of the single $x$ component of the vector $\bar{H}$ depends only on the two spatial dimensions $y$ and $z$. Equation (12) is a valid solution in both the straight and curved duct since it identically satisfies Maxwell's divergence equations for magnetic fields.

Substituting equation (12) into equation (11) and performing the required manipulation yields

$$\frac{\partial}{\partial y}\left(\frac{1}{\varepsilon_y}\frac{\partial H_x}{\partial y}\right) + \frac{\partial}{\partial z}\left(\frac{1}{\varepsilon_T}\frac{\partial H_x}{\partial z}\right) + \omega^2 \mu_r H_x = 0 \tag{13}$$

In vector form,

$$\nabla \bullet \frac{1}{\varepsilon} \nabla H_x + \omega^2 \mu_r H_x = 0 \tag{14}$$

Equation (14) represents the governing wave equation to be solved by finite-element theory.

## UNIFORM DUCT ANALYTICAL SOLUTIONS

The analytical solutions of equation (14) for wave propagation in the uniform perfectly conducting duct having an anechoic entrance and exit will be employed to give the termination boundary condition for the finite-element region. The analytical solution of equation (14) for TM waves traveling between perfectly conducting parallel plates is given as (ref. 3, p. 458):

$$H_{xa} = \sum_{n=1}^{N_m} A_n^+ \cos\left(\frac{(n-1)\pi}{b_a} y\right) e^{-jk_{zn}z} + \sum_{n=1}^{N_m} A_n^- \cos\left(\frac{(n-1)\pi}{b_a} y\right) e^{+jk_{zn}z} \tag{15}$$

For the $e^{j\omega t}$ time dependence used here, the $A_n^+ e^{-jk_{zn}z}$ term represents a wave propagating in the positive $z$ direction while the $A_n^- e^{jk_{zn}z}$ term represents a wave moving in the negative $z$ direction.

The axial wave number $k_{zn}$ in equation (15) is

$$k_{zn} = + k \sqrt{1 - \left(\frac{(n-1)\pi}{b_a k}\right)^2} \qquad \left(\frac{(n-1)\pi}{b_a k}\right) \leq 1 \tag{16}$$

$$k_{zn} = -jk \left| \sqrt{\left(\frac{(n-1)\pi}{b_a k}\right)^2 - 1} \right| \qquad \left(\frac{(n-1)\pi}{b_a k}\right) > 1 \tag{17}$$

A similar solution exists at the exit, except only positive going waves are considered.

$$H_{xb} = \sum_{n=1}^{N_m} B_n^+ \cos\left(\frac{(n-1)\pi}{b_b} y\right) e^{-jk_{zn}z} \tag{18}$$

## BOUNDARY CONDITIONS

A variety of boundary conditions will be used in the finite-element solution of equation (14) for the model problem which is displayed in schematic

form in figure 2. Each of the required conditions will now be briefly discussed.

## Input Condition

The analysis assumes a given number $N_m$ of propagating $A_n^+$ modes (eq. 15). These modes effectively set the level of the magnetic field in the finite-element region and can be viewed as the equivalent Dirichlet boundary conditions required for elliptic boundary value problem as defined by equation (14).

The modal expression represented by equation (15) has been truncated to a total of $N_m$ modes of the infinite number possible. Thus, a total of $N_m$ unknown modal amplitudes $A_1^-$, $A_2^-$, . . . $A_{N_m}^-$ have been introduced. $N_m$ constraint equations will be required to determine each of these unknown reflection coefficients. The equations used to define these coefficients will now be introduced.

## Continuity at Inlet and Exit

The tangential component of an $H$ field is continuous across an interface between two physically real media which are not perfect conductors (ref. 4, eq. (1.61)). Thus, the boundary condition becomes

$$H_{xa} = \tilde{H}_x \quad (z = 0; \quad 0 < y < b_a) \tag{19}$$

where $H_{xa}$ is the modal representation of magnetic field in the analytical inlet region given by equation (15) and $\tilde{H}_x$ represent the finite-element approximation for $H_x$ at the interface. The hat over $\tilde{H}_x$ implies an approximate finite element numerical solution to be discussed in detail in a following section.

At the inlet to the curved section, shown in figure 2, the $H_{xa}$ in the analytical region given by equation (15) must match the magnetic field defined by the finite-element nodal points along the boundary interface. Many possible matching methods can by employed for this boundary condition, such as point collocation, least squares, or weighted residuals. A weighted residual approach was used herein with the weighting function equal to the eigenfunctions for the uniform infinitely long duct with perfectly conducting walls;

$$\int_0^{b_a} \left[H_{xa}(y) - \tilde{H}(y)\right] \cos\left(\frac{(m-1)\pi y}{b_a}\right) dy = 0 \quad \text{at } z = 0 \tag{20}$$

($N_m$ equations, $m = 1,2,3, N_m$)

Equation (20) represents $N_m$ separate equations; one for each coefficient defined in equation (15). The symbol $m$ has been introduced as a dummy variable to make it distinct from the multiple $n$ mode numbers that make up the $H_a$ analytical function. A similar equation exists at the exit.

In addition to the tangential component of the magnetic field, the tangential component of the electric field must also be continuous across the interface (ref. 3, eq. (7-52(a))). Using equation (4) to express the tangential electric field in terms of the magnetic field (ref. 5, eq. (7-4)) yields

$$\frac{1}{\varepsilon}\frac{\partial \tilde{H}_x}{\partial z} = \frac{1}{\varepsilon_a} = \frac{\partial H_{xa}}{\partial z} \tag{21}$$

The weak form of the finite-element solution will be employed in the solution of this problem. In this form, a contour integral term will be developed which will contain a natural boundary condition of the form $\nabla\tilde{H} \cdot \bar{n}$ where $\bar{n}$ represents the unit outward normal. Equation (21) can be expressed in this gradient form at the entrance as

$$\nabla\tilde{H}_x \cdot \bar{n} = \frac{-\varepsilon}{\varepsilon_a}\frac{\partial H_{xa}}{\partial z} \text{ (inlet)} \tag{22}$$

and at the exits

$$\nabla\tilde{H}_x \cdot \bar{n} = \frac{+\varepsilon}{\varepsilon_b}\frac{\partial H_{xb}}{\partial z} \text{ (exit)} \tag{23}$$

The sign change in equations (22) and (23) comes directly from the directional change of the unit outward normal $\bar{n}$.

## Perfectly Conducting Wall Conditions

At a perfectly conducting wall, the tangential component of the electric field vector is zero (ref. 3, eq. (7-52(a)) or ref. 4, eq. (1.69)). Again, using equation (4) to relate the electric field to the magnetic field (ref. 5, eq. (7-4)), the component of the gradient of the magnetic field normal to a perfectly conducting wall becomes

$$\nabla\tilde{H}_x \cdot \bar{n} = 0 \tag{24}$$

## FINITE-ELEMENT THEORY

The finite-element formulation of the electromagnetic wave equation is now generated by using the method of weighted residuals to obtain an integral form of the variable property wave equation over the whole (global) domain $D$ shown in figure 3.

## System Discretization

The continuous domain $D$ is first divided into a number of discrete areas staked out by the nodal points as shown in figure 2.

## Global Weighted Residual Approach

In the classical weighted residual manner, the magnetic field intensity component $\tilde{H}_x(y,z)$ is curve fitted by expanding in terms of all the unknown nodal values $H_{xi}(y_i,z_i)$ and a known series of basis (weight) functions, such that

$$\tilde{H}_x(y,z) = \sum_{i-1}^{N} W_i(y,z)H_{xi} = [W]\{H_x\} \tag{25}$$

where the basis or weight functions $W_i(y,z)$ characterizes the spatial dependence of $\tilde{H}_x(y,z)$ in terms of $H_{xi}$ which represents the unknown value of the magnetic field intensity component at the $i^{th}$ nodal point in the global region. As before in equation (19), the hat over the $H_x(y,z)$ indicates that it is the approximate numerical solution to $H_x(y,z)$. The precise form of the known weight which will be employed in this analysis will be presented later in the section entitled Galerkin Approximation.

Upon substituting the assumed magnetic field series, equation (25), into the governing wave equation at each nodal point, a distribution of errors results throughout the finite-element region due to the approximate nature of the assumed series. In accordance with the method of weighted residuals, the integral of the assumed basis function $W_i$ and the error at each nodal point are forced to be zero (orthogonal) by letting

$$\iint_D W_i \left( \nabla \bullet \frac{1}{\varepsilon} \nabla \tilde{H}_x + \omega^2 \mu_r \tilde{H}_x \right) dydz = 0 \tag{26}$$

$$(i = 1,2, \ldots N \text{ equations})$$

Thus, there are $N$ separate equations (written in compact form); one equation for each of the $N$ nodal $H_{xi}$ unknowns.

By making use of the gradient vector identity of a scalar and a vector and Green's theorem in a plane (ref. 7, p. 79, eq. (4.7(b))) equation (26) can be converted to

$$\int_D \left[ \frac{1}{\varepsilon} \nabla W_i \bullet \nabla \tilde{H}_x - W_i \omega^2 \mu_r \tilde{H} \right] dydz - \oint_S \left( W_i \frac{1}{\varepsilon} \nabla \tilde{H}_x \bullet \bar{n} \right) ds = 0 \tag{27}$$

$$(i = 1,2, \ldots N \text{ equations})$$

In effect, the second order differential equation has been reduced to a first order equation allowing the use of the weak formulation of the finite-element theory.

## Finite Element Approximation

Equation (27) is valid over the entire domain $D$ shown in figure 3 or any subdomain $A_e$, as represented by the area of a small triangular element embedded in the region as depicted in figure 3. To begin the finite-element aspect of the weighted residual method, the domain $D$ is assumed to be divided into $M$ elements defined by $N$ nodes, see figure 2. In this case, equation (27) can be written as

$$\sum_{e=1}^{M} \iint_{Ae} \left( \frac{1}{\varepsilon_e} \nabla W_i \bullet \nabla \tilde{H}_x^{(e)} - W_i \omega^2 \mu_{re} \tilde{H}_x^{(e)} \right) dydz - \oint_S \left( W_i \frac{1}{\varepsilon_e} \nabla \tilde{H}_x^{(e)} \bullet \bar{n} \right) ds = 0$$

$$(i = 1,2 \ . \ . \ . \ N \ \text{equations}) \qquad (28)$$

Where the properties are now given a subscript $e$ to indicate that they may vary from element to element. Although the area integration in equation (28) applies to an individual element, the line integral is still defined over the global surface area, and as such, can be treated independently from the local area integrations. Also, $\tilde{H}_x$ has been replaced by $\tilde{H}_x^{(e)}$ which expresses the magnetic field in terms of the three local element nodes associated with each triangular element as shown in figure 3.

## Galerkin Approximation

In the method of weighted residuals, the weight $W_i$ is assumed to be a known function which has the property of being unity at node $i$ and identical to zero at all other nodes. The Galerkin approximation to the more general weighted residual approach assumes that $W_i$ can be related to local shape function $N_i^{(e)}(x,y)$ which represents the variation of the field variable $H_x$ and its derivatives inside the element.

The form of the local shape matrix $[N]^{(e)}$ depends on the type of element used. For the linear triangular element employed herein, the known value of $N^{(e)}$ can be found in texts on finite elements (ref. 9, p. 6). Thus, the magnetic field $\tilde{H}_x(y,z)$ inside a particular element can be expressed in terms of the local shape function $N_i(y,z)$ as follows:

$$\tilde{H}_x(y,z) \cong \tilde{H}_x^{(e)}(y,z) = N_1^{(e)}(y,z)H_{x1}^{(e)} + N_2^{(e)}(y,z)H_{x2}^{(e)} + N_3^{(e)}(y,z)H_{x3}^{(e)}$$

$$= \sum_{j=1}^{3} N_j^{(e)} H_{xj}^{(e)} = [N]^{(e)} \{H_x\}^{(e)} \qquad (29)$$

where $\{H_x\}^{(e)}$ is the vector of nodal values of $H_x$ for a general element e with subscripts 1, 2, and 3 representing the nodal positions as shown in figure 3. The subscripts 1, 2, and 3 take on the actual nodal number of figure 2 when applied to a specific element in the finite-element region.

The weight $W_i(y,z)$ is now approximated by multiple values of $N_i^{(e)}$.

$$W_i(y,z) = N_i^{(e)}(y,z) \tag{30}$$

in all elements containing the $i^{th}$ node. For all elements which do not contain the node i, the weight $W_i$ is assumed zero not only at all other nodes (as required by the general definition of $W_i$) but also at all values of y and z in the elements which do not contain the node i. Thus, $W_i$ can be visualized as a multisided pyramid on a flat surface with its apex over node i and corners at adjacent nodes.

Recognizing that $N_i^{(e)}$ is zero for all elements not having the unknown $H_{xi}$ associated with a particular element, the finite element equation (28) can now be written in compact form as

$$\sum_{e=1}^{M} \iint_{Ae} \left( \frac{1}{\varepsilon_e} \nabla N_i^{(e)} \bullet \nabla \tilde{H}_x^{(e)} - N_i^{(e)} \omega^2 \mu_{re} \tilde{H}_x^{(e)} \right) dydz$$

$$- \oint_S \left( N_i^{(e)} \frac{1}{\varepsilon_e} \nabla \tilde{H}_x^{(e)} \bullet \bar{n} \right) ds = 0 \tag{31}$$

(i = 1,2, . . . N equations)

## Global Matrix

The finite-element aspects of converting equation (31), the entrance condition (20), and the similar exit condition into a set of global difference equations can be found in text books as well as reference 10 and for conciseness will not be presented herein. However, equation (70) of reference 10 is identical to equation (31). In reference 10, additional details can be found for the manipulation of equation (31) into the final finite-element solution.

## RESULTS AND COMPARISONS

For theory and code validation, the finite-element solution is first applied to a straight walled case where a simple exact solution exists. Next, the solution is applied to a mitred duct approximation to an S-duct for which certain results can be expected from previous numerical solutions. As a third example, the finite-element solutions will be presented for a set of S-ducts of various lengths with perfectly conducting boundary conditions. Finally, the solution for a curved duct with an absorbing wall will be presented. With the exception of the first example, all ducts are air filled ($\varepsilon = \varepsilon_r = 1$, $\mu_r = 1$).

### Example 1: Reflection and Transmission with Normal Incidence

Consider the case of an incident plane magnetic wave $H_x$ of dimensionless frequency $2\pi$ encountering a step change in the dielectric constant from 1 to 4 at the dimensionless axial position of $z$ equal to 0.25 inside the finite-element grid. As shown in figure 4, the finite element and exact analytical (ref. 5, chapter 5) theories are in good agreement for the absolute magnitude of the magnetic intensity $H_x$. Additional validation examples for propagation with straight walls can be found in reference 10.

### Example 2: Double Mitre Approximation to S-Duct

As shown in figure 5, a double 90° mitred duct can be represented as a rough approximation to an S-duct. Plane wave acoustic propagation in a single 90° mitred duct is well understood from the numerical studies of Shepherd and Cabelli (ref. 11). The energy reflection coefficient of a single 90° mitred bend for plane wave incidence is shown in figure 6 from reference 11. As the frequency of the incoming plane acoustic wave approaches the first mode cut-on frequency, the transmitted mode shape in the exit portion of the mitred duct approaches the shape of the first higher order mode. Consequently, as shown in figure 6, nearly all the incoming energy is reflected back down the duct, since the transmitted wave is cut-off and cannot carry energy. For very low frequency nearly all its energy is transmitted down the duct while at higher frequencies complete reflection of energy is expected, as depicted by the ray approximation shown in figure 6.

As seen in figures 5 and 7, combining two 90° mitred ducts produces a rough approximation for an S-duct. As shown in figure 7, the rear and forward faces have been fitted with a steep S-curve. The modified double mitred duct has roughly the same characteristic as the single mitred duct, as seen in figure 7. The energy reflection coefficient approaches unity near the first cut-off (but slightly less), at low frequencies the wave is passed unattenuated, and at higher frequencies the reflection coefficient is near unity. In addition, a low frequency hump appears at a frequency of $\omega$ near 1.5. Perhaps the duct is now acting analogously to an acoustic expansion chamber at low frequency which has similar types of humps due to resonance effects (ref. 12, p. 8).

### Example 3: S-Duct

In the third example, the energy reflection coefficient was determined for the S-duct shown in figure 8 for various lengths. Generally, as the length increases the reflected energy decreases. In contrast to the mitred duct, the reflected energy approaches a minimum at the first node cut-on frequency of 3.14. Again, at the lower frequencies, the energy is nearly all transferred down the duct. The energy flux was determined by calculating the Poynting vector in the inlet and outlet duct from the calculated modal coefficients.

## Example 4: Wall Absorbers

Figure 9 shows duct configurations with an absorbing region along the upper and lower walls of the duct. Figure 9(a) show the straight wall configuration while figure 9(b) shows the curved wall configuration. For the same absorbing material, the attenuation of both ducts will be compared. The wall material will have a relative permeability of 4.1 and a complex permittivity of 1-j2.83. An incident plane wave of dimensionless frequency $\omega$ of $2\pi$ is assumed. Figure 10 displays the finite-element grid used for both configurations.

For the straight duct, the axial component of the energy level (Poynting vector) is shown in figure 11. The drop in level is due to grazing absorption by the walls. Figure 12 displays contour plots of the magnitude of the magnetic field for the straight duct absorber configuration. The solid line drawing shows the complete contours, while the symbols are plotted at selective points in the companion figure so that the actual magnitude of the contour can be readily determined. For convenience the magnitude of the magnetic field has been renormalized between 0 and 1 according to the formula

$$\left|H_{x_{contour}}\right| = \frac{\left|H_x\right| - \left|H_{xmin}\right|}{\left|H_{xmax}\right| - \left|H_{xmin}\right|} \tag{32}$$

where $H_{xmax}$ is the maximum value of magnitude of the magnetic field in the plotting domain and $H_{xmin}$ is the minimum value of $H_x$ in the plotting domain.

As seen in figure 12, the magnetic field has decreased to near zero at the walls but remains relatively high in the center of the duct. In effect, electromagnetic energy beams through the center of the duct. This should not occur in the curved duct, because a more normal type impingement absorption will take place.

For the curved duct, the axial component of the energy level is shown in figure 13. For the straight duct, the decrease in duct exit power due to wall absorption was -3.73 dB, while for the curved duct the decrease in exit energy due to wall absorption and reflection was -18.5 dB. The reflected energy at the inlet due to the change in duct curvature and wall impedance was -13.4 dB. The drop in energy level at the exit of the curved duct is considerably larger than the straight duct due to the more normal incidence of the magnetic field on the absorbing walls. Figure 14 displays the magnetic field contours. In this case, the curved wall prevents the beaming down the center which occurs in a straight duct. Consequently, the magnetic field quickly damps to near zero.

## CONCLUDING REMARKS

A finite-element Galerkin formulation was developed to study transverse magnetic (TM) wave propagation in two-dimensional curved S-shaped ducts with both perfectly conducting and absorbing walls. The derivations from Maxwell's equations assumed that the material properties could vary with position resulting in a nonhomogeneous variable property two-dimensional wave equation. This eliminated the necessity of finding the boundary conditions between the different materials. Consequently, a complex structure can be easily modeled

simply by changing the property of elements in the finite-element domain. The reflection and transmission at the entrance and the exit of the curved duct are determined exactly by coupling the finite-element solutions in the curved duct to the eigenfunctions of an infinite, uniform, perfectly conducting duct.

The numerical formulation is relatively simple to use and appears to give very accurate results. Example solutions are presented for a doubled mitred and S-duct of various lengths and with perfectly conducting and absorbing duct walls. The length of the S-duct is found to significantly affect the reflective characteristics of the duct. Also, wall curvature is shown to greatly enhance the absorption properties of a duct.

## REFERENCES


1. G. Kennedy, Electronic Communication Systems, 3rd ed., New York: McGraw-Hill, 1985.

2. K.J. Baumeister, W. Eversman, R.J. Astley, and J.W. White, "Acoustics in Variable Area Duct: Finite Element and Finite Difference Comparison to Experiment," AIAA J., vol. 21, pp. 193-199, 1983.

3. D.K. Cheng, Field and Wave Electromagnetics, Reading, MA: Addison-Wesley, 1983.

4. M.B. Kraichman, Handbook of Electromagnetic Propagation in Conducting Media, NAVMAT P-2302, Washington, D.C.: U.S. Government Printing Office, 1970.

5. E.C. Jordan and K.G. Balmain, Electromagnetic Waves and Radiating Systems, 2nd ed., Englewood Cliffs: Prentice-Hall, 1968.

6. S.V. Patankar and T.M. Shih, Numerical Heat Transfer and Fluid Flow, New York: McGraw-Hill, 1980.

7. H.C. Martin and G.F. Carey, Introduction to Finite Element Analysis, New York: McGraw-Hill, 1973.

8. H.C. Lester and T.L. Parrott, "Application of a Finite Element Methodology for Computing Grazing Incidence Wave Structure in an Impedance Tube: Comparison with Experiment," AIAA Paper 79-0664, Mar. 1979.

9. P.P. Silvester and R.L. Ferrari, Finite Elements for Electrical Engineers, Cambridge, England: Cambridge University Press, 1983.

10. K.J. Baumeister, "Finite Element Analysis of Electromagnetic Propagation in an Absorbing Wave Guide," NASA TM-88866, 1986.

11. I.C. Shepherd and A. Cabelli, Transmission and Reflection of Higher Order Acoustic Modes in a Mitred Duct Bend, J. Sound Vibration, vol. 77, pp. 495-511, 1981.

12. D.D. Davis, Jr., G.M. Stokes, D. Moore, and G.L. Stevens, Jr., Theoretical and Experimental Investigation of Mufflers with Comments on Engine-Exhaust Muffler Design, NACA Report 1192, 1954.

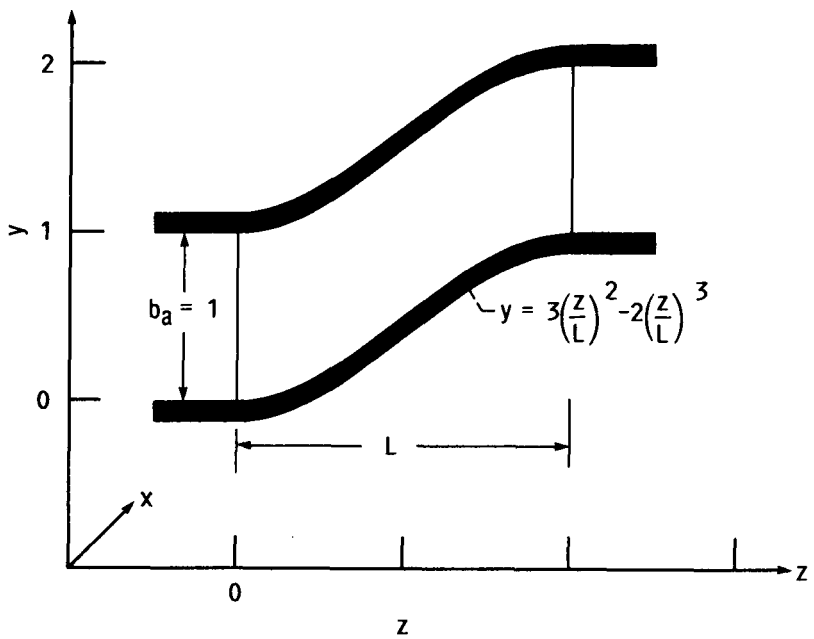


FIGURE 1. - S-DUCT GEOMETRY AND COORDINATE SYSTEM.

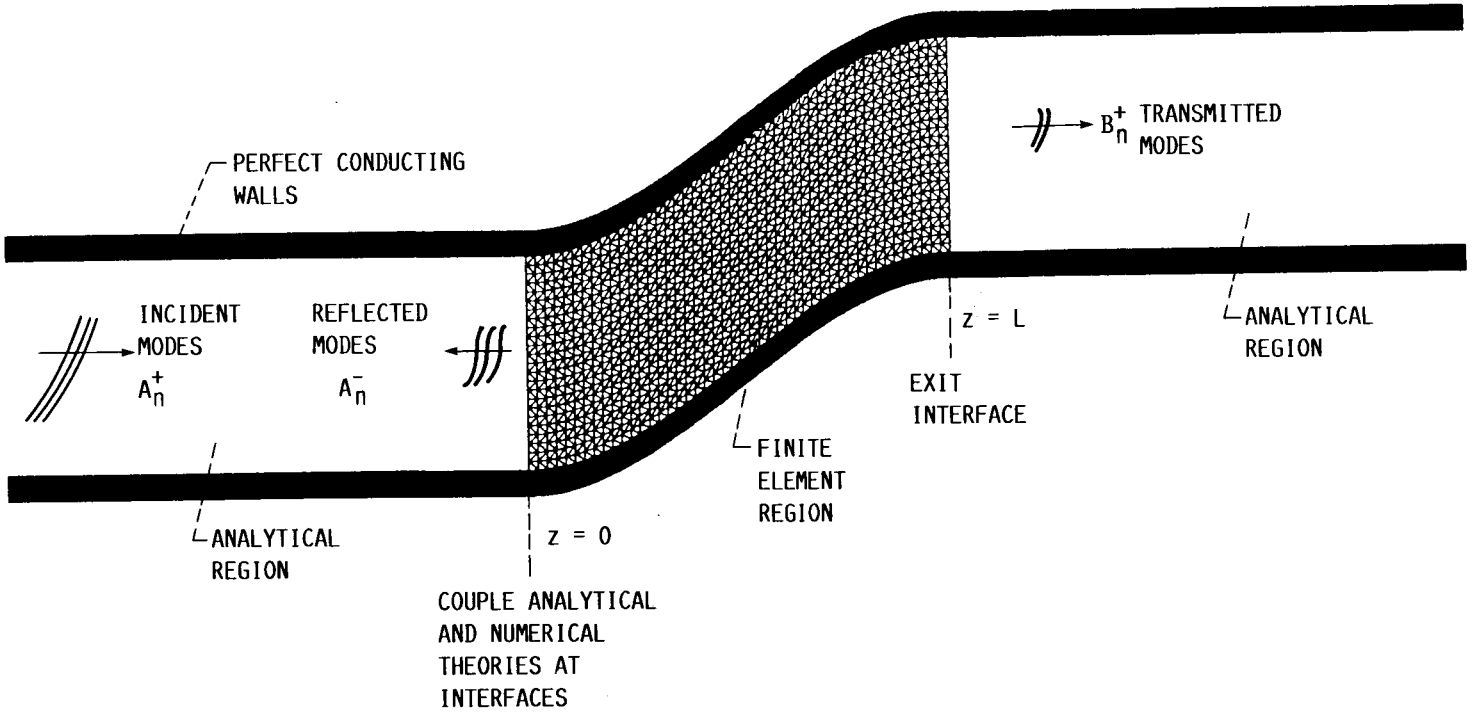


FIGURE 2. - TWO DIMENSIONAL S-DUCT FINITE ELEMENT MODEL.

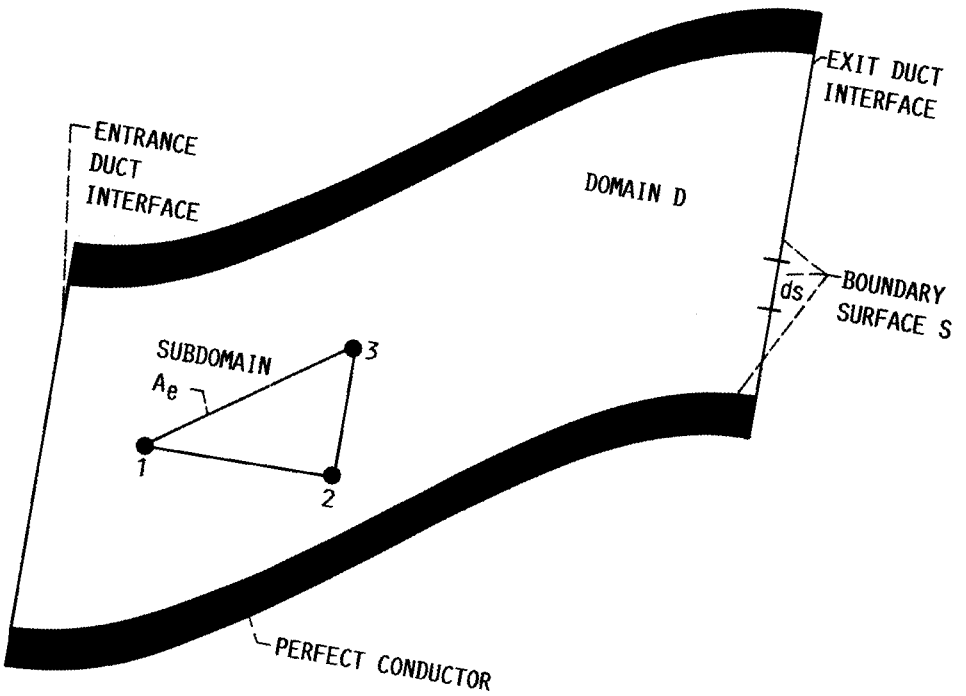


FIGURE 3. - ELECTROMAGNETIC BOUNDARY VALUE FORMULATION.

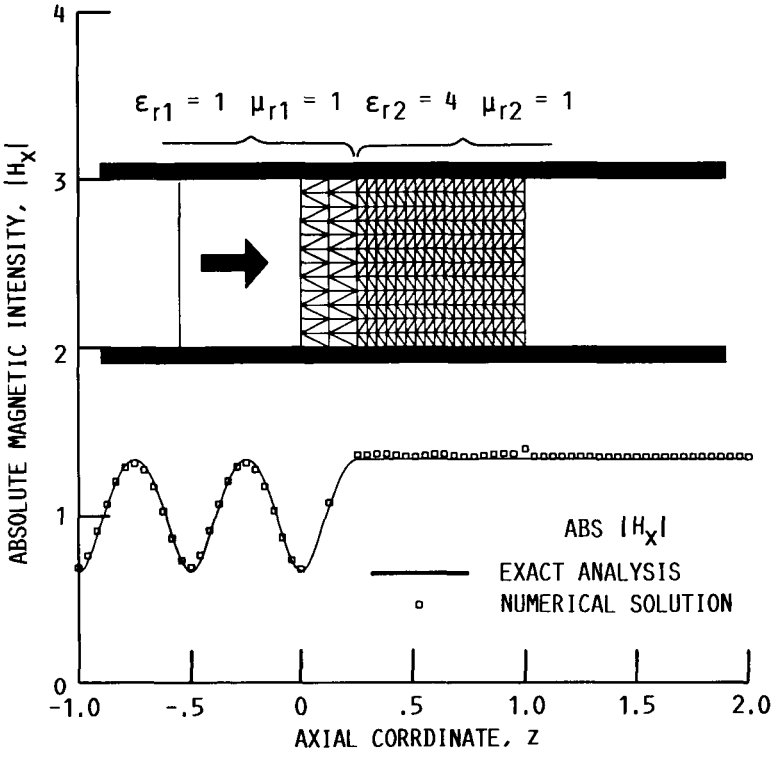


FIGURE 4. - A COMPARISON OF THE MAGNITUDE OF THE AXIAL MAGNETIC INTENSITY VARIATION ALONG THE LOWER WALL IN A UNIFORM DUCT WITH PERFECTLY CONDUCTING WALLS AND A CHANGE IN PROPERTIES OF THE MEDIA AT z OF 0.25 ($\varepsilon_{r1}$ = 1.0 AND $\varepsilon_{r2}$ = 4.0) AS OBTAINED BY USING AN EXACT SOLUTION AND A FINITE ELEMENT SOLUTION FOR A PLANE WAVE (MODE-ONE) INCIDENT AT z = 0 WITH $\omega = 2\pi$.

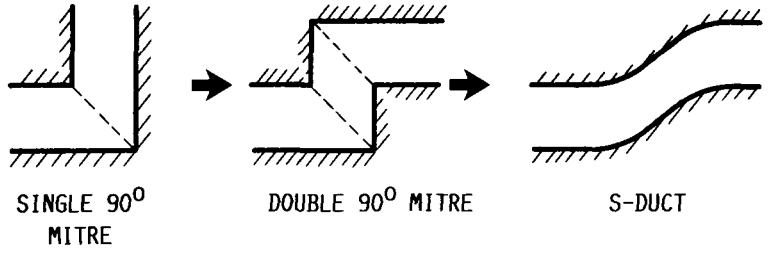


FIGURE 5. - DOUBLE MITRE APPROXIMATION TO S-DUCT.

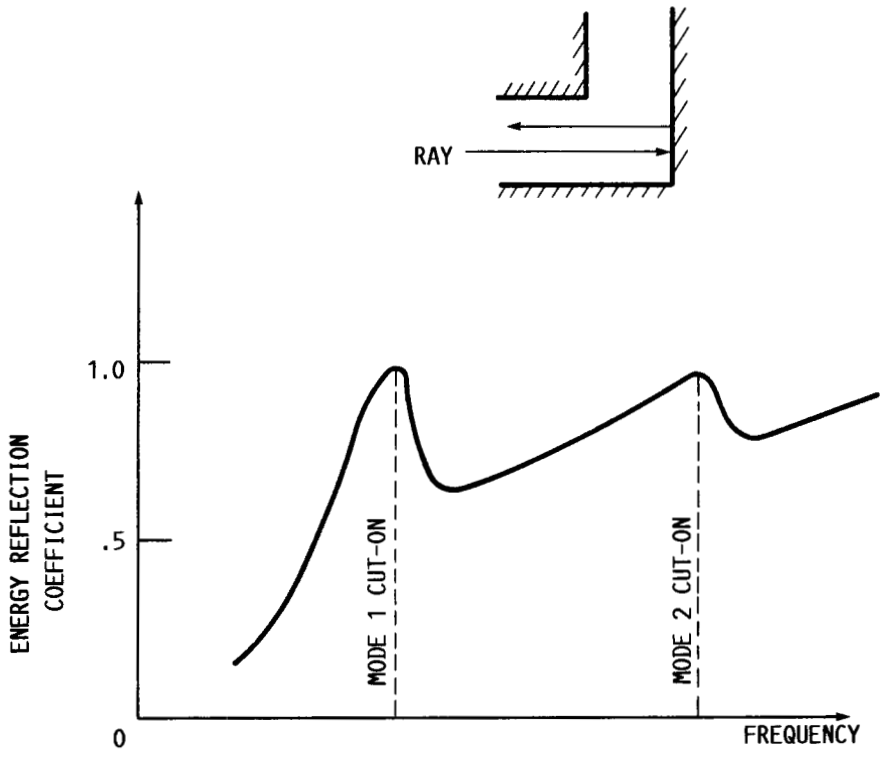


FIGURE 6. - ENERGY REFLECTION COEFFICIENT OF $90^{o}$ MITRED BEND FOR PLANE WAVE INCIDENCE AS A FUNCTION OF FREQUENCY (REF. 11).

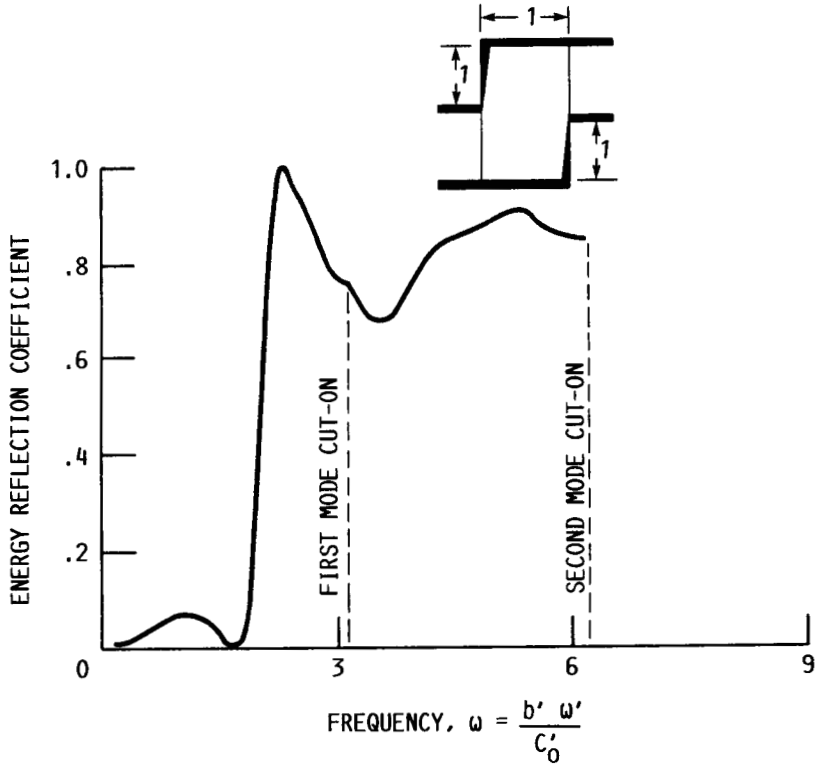


FIGURE 7. - ENERGY REFLECTION COEFFICIENT OF DOUBLE MITRE APPROXIMATION TO S-DUCT FOR PLANE WAVE INCIDENCE AS A FUNCTION OF FREQUENCY.

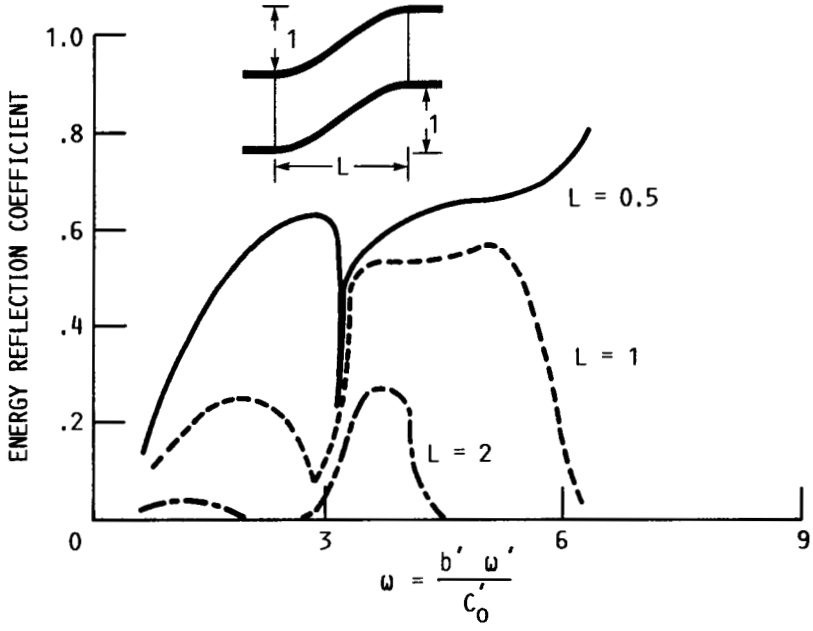


FIGURE 8. - ENERGY REFLECTION COEFFICIENT OF S-DUCT FOR PLANE WAVE INCIDENCE AS A FUNCTION OF FREQUENCY.

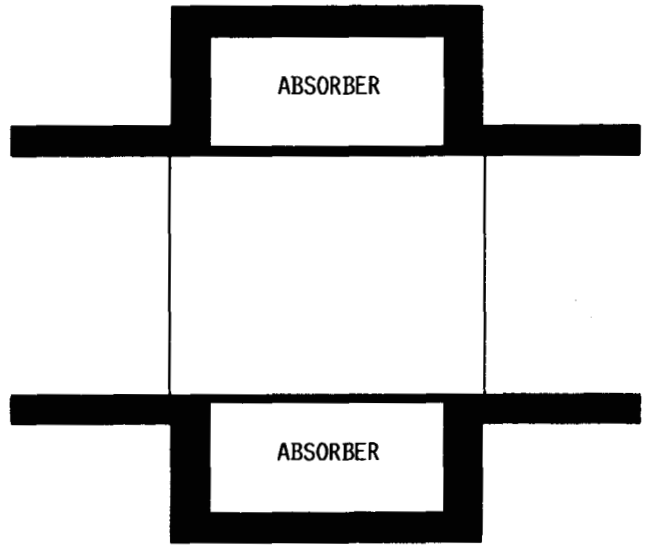


(A) STRAIGHT DUCT.

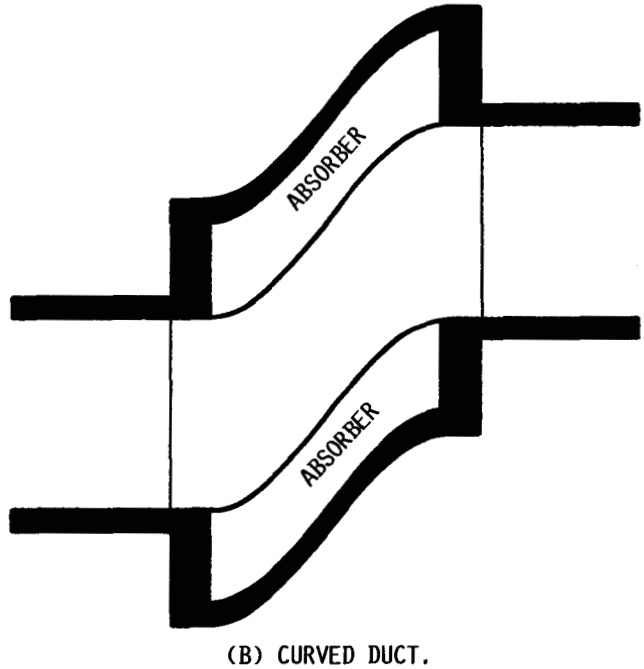


(B) CURVED DUCT.

FIGURE 9. - ABSORBING WALL DUCT CONFIGURATIONS.

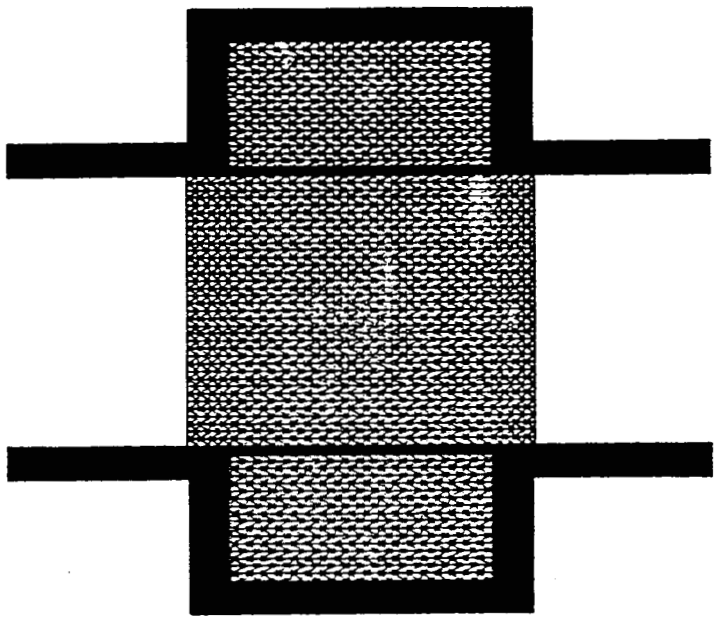

(A) STRAIGHT DUCT.

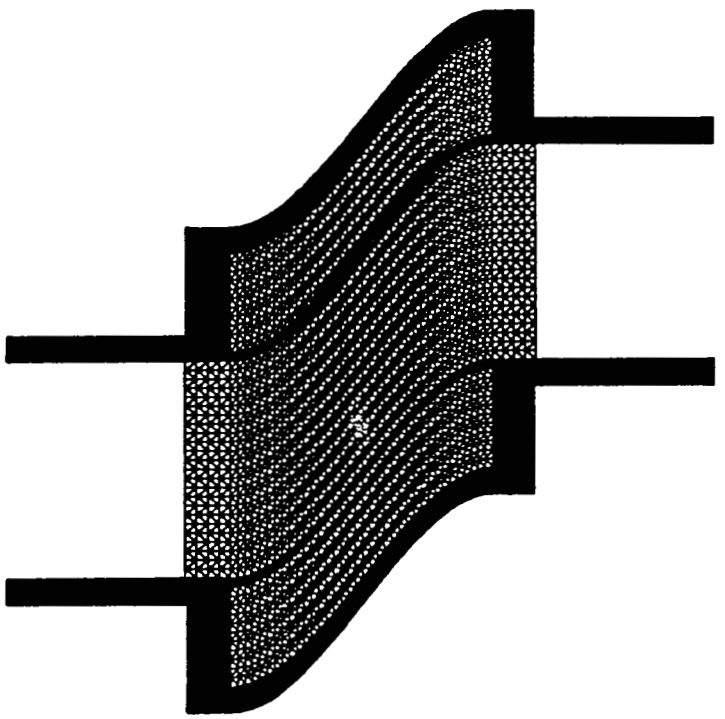

(B) CURVED DUCT.

FIGURE 10. - DISCRETIZATION OF AIR FILLED WAVE GUIDE WITH ABSORBERS MOUNTED ALONG BOTH UPPER AND LOWER WALLS.

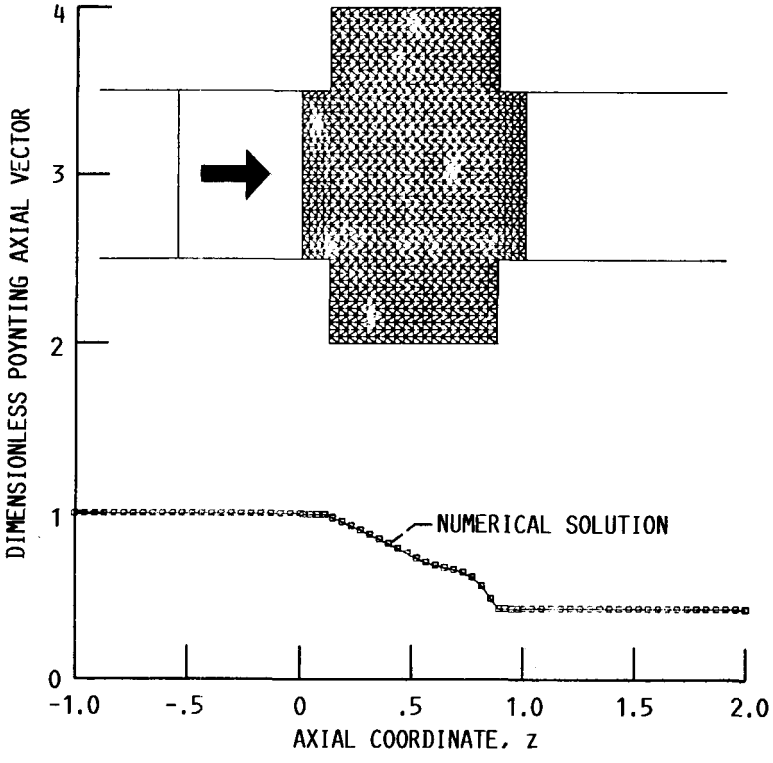


FIGURE 11. - EFFECT OF UPPER AND LOWER WALL ABSORBERS ON THE MAGNITUDE OF THE AXIAL FLUX OF ENERGY (POYNTING VECTOR) FOR A FIVE-MODE MODAL EXPANSION IN THE ENTRANCE AND EXIT DUCTS.

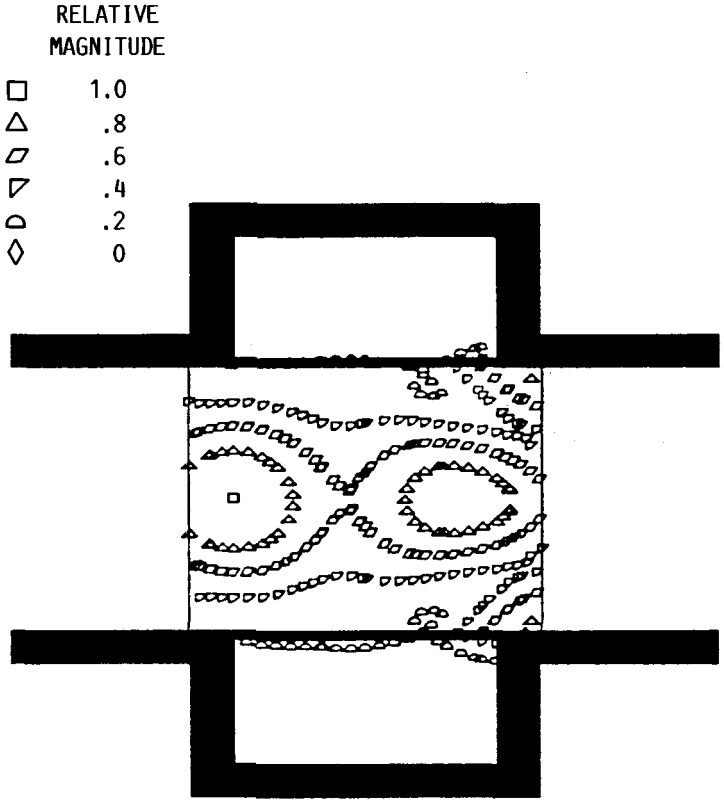


FIGURE 12. - CONTOUR PLOTS OF MAGNETIC FIELD AMPLITUDE.

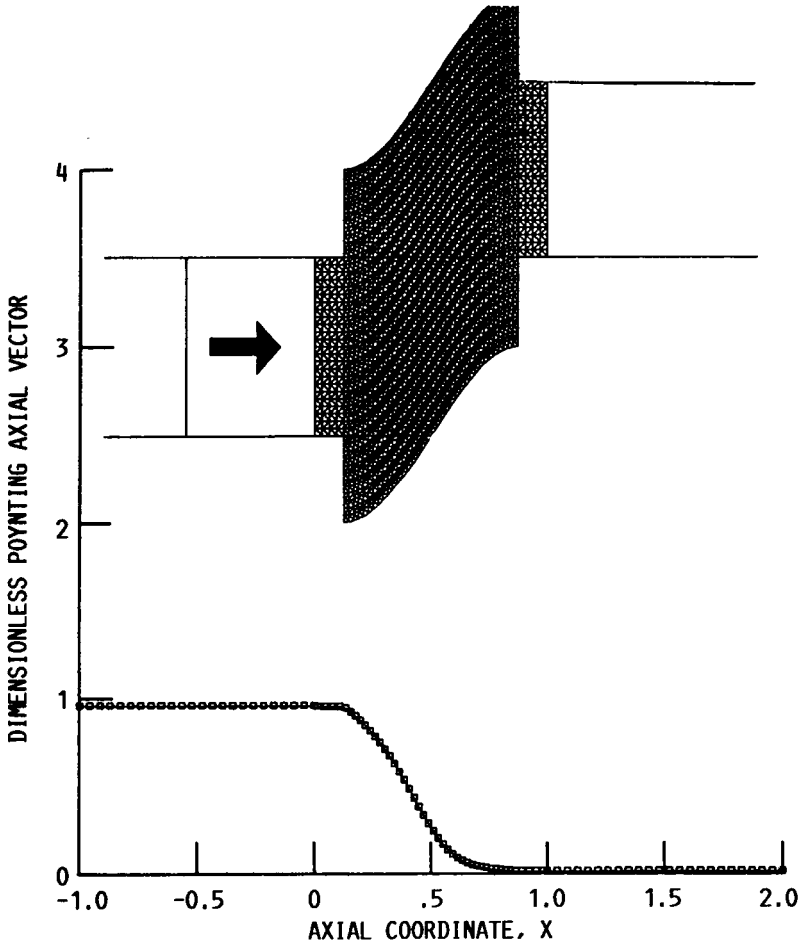


FIGURE 13. - EFFECT OF UPPER AND LOWER WALL ABSORBERS ON THE MAGNITUDE OF THE AXIAL FLUX OF ENERGY (POYNTING VECTOR) FOR A FIVE-MODE MODAL EXPANSION IN THE ENTRANCE AND EXIT DUCTS.

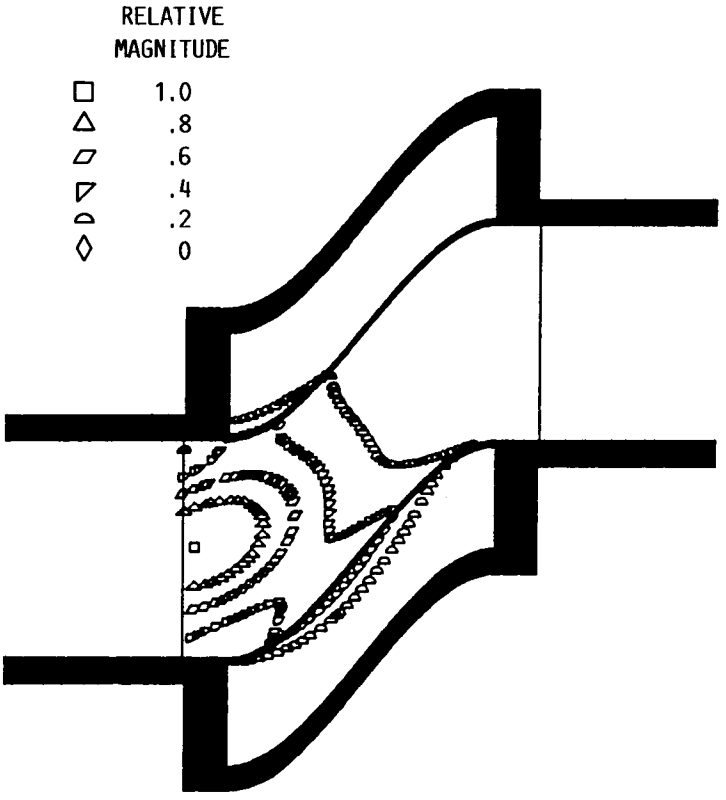


FIGURE 14. - CONTOUR PLOTS OF MAGNETIC FIELD AMPLITUDE.

NASA
National Aeronautics and Space Administration

# Report Documentation Page

| 1. Report No. | 2. Government Accession No. | 3. Recipient's Catalog No. |
|---|---|---|
| NASA TM-100833 | | |

**4. Title and Subtitle**

Electromagnetic Propagation in PEC and Absorbing Curved S-Ducts

**5. Report Date**

**6. Performing Organization Code**

**7. Author(s)**

Kenneth J. Baumeister

**8. Performing Organization Report No.**

E-3507

**10. Work Unit No.**

505-62-21

**9. Performing Organization Name and Address**

National Aeronautics and Space Administration
Lewis Research Center
Cleveland, Ohio 44135-3191

**11. Contract or Grant No.**

**13. Type of Report and Period Covered**

Technical Memorandum

**12. Sponsoring Agency Name and Address**

National Aeronautics and Space Administration
Washington, D.C. 20546-0001

**14. Sponsoring Agency Code**

**15. Supplementary Notes**

Prepared for the 1988 IEEE AP-S International Symposium and URSI Radio Science Meeting, Syracuse, New York, June 6-10, 1988.


**16. Abstract**

A finite-element Galerkin formulation has been developed to study transverse magnetic (TM) wave propagation in two-dimensional S-curved ducts with both perfectly conducting and absorbing walls. The reflection and transmission at the entrances and the exits of the curved ducts are determined by coupling the finite-element solutions in the curved ducts to the eigenfunctions of an infinite, uniform, perfectly conducting duct. Example solutions are presented for a double mitred and S-ducts of various lengths. The length of the S-duct is found to significantly effect the reflective characteristics of the duct. Also, the effect of curvature on an absorbing duct wall is illustrated.



**17. Key Words (Suggested by Author(s))**

Finite element
Curved duct
Electromagnetics

**18. Distribution Statement**

Unclassified - Unlimited
Subject Category 32

| 19. Security Classif. (of this report) | 20. Security Classif. (of this page) | 21. No of pages | 22. Price* |
|---|---|---|---|
| Unclassified | Unclassified | 26 | A03 |

NASA FORM 1626 OCT 86

*For sale by the National Technical Information Service, Springfield, Virginia 22161